Int. J. Electrochem. Sci., 14 **(2019)** 7317 – 7331, doi: 10.20964/2019.08.82

International Journal of
ELECTROCHEMICAL
SCIENCE
www.electrochemsci.org

Preparation of Mission Grass Flower-Based Activated Carbon Monolith Electrode for Supercapacitor Application

E. Taer[1,], R. Taslim[2], W. S. Mustika[1,3], S. Nurjanah[1], R. I. Yani[1], Y. P. Sari[1], H. Yusra[1], Awitdrus[1], Apriwandi[1], Agustino[1], D. Tahir[4]*

[1] Department of Physics, University of Riau, 28293 Simpang Baru, Riau, Indonesia.
[2] Department of Industrial Engineering, Islamic State University of Sultan Syarif Kasim, 28293 Simpang Baru, Riau, Indonesia.
[3] Department of Physics, Institute Technology of Bandung, Bandung, West Java, Indonesia
[4] Department of Physics, Hasanudin University, Makassar, South Sulawesi, Indonesia
[*]E-mail: eman.taer@yahoo.com

Received: 6 April 2019 / *Accepted:* 2 June 2019 / *Published:* 30 June 2019

The preparation and characterization of an activated carbon monolith for supercapacitor application created from mission grass flowers was performed. The benefits of carbon electrode monolith production from mission grass flowers include the low cost of the raw material and smooth structures that can bind without the use of an adhesive. Carbon electrode preparations were evaluated with respect to several aspects: chemical activating agent, carbonization temperature, and physical activation temperature and particle size. These aspects represent several main aspects in the production of carbon electrodes. The primary characterization required to determine carbon electrode properties is based on the specific surface area and capacitance. Our characterization found that a carbon electrode monolith manufactured from mission grass flowers had a maximum surface area of 950 m^2 g^{-1} and a maximum specific capacitance of 120 F g^{-1}. In addition, the crystallinity and morphology of the monolith's surface properties were tested and analysed.

Keywords: Mission grass; carbon electrode; specific capacitance; supercapacitor

1. INTRODUCTION

Carbon is a functional material that has been widely studied in recent years. The material's excellent physical and chemical properties lend themselves to a variety of shapes and sizes. Thus, carbon is used in many fields [1]. Another advantage is the availability of abundant raw material, which means that production costs are relatively low. One source used in the production of carbon is biomass [2-4]. For example, plantations and other forms of sustainable agriculture are abundant sources of biomass. In Indonesia, oil palm, rubber, paddy, coconut and corn farming produces

substantial amounts of biomass. Biomass can also be obtained from clearing land of grass. Grasses are frequently used as source material in the production of carbon with a relatively low cost. Mission grass *(Pennisetum polystachion)* is the most widely found grass in Indonesia. Its availability in large quantities and free of charge are advantages to its use in carbon production. Several reports mention that mission grass has been used as a fodder source and processed to produce bioethanol [4-5]. In this study, the use of mission grass flowers as a novel material in the production of carbon electrodes for supercapacitor application is investigated.

A supercapacitor, also known as a double-layer capacitor, is a type of electrical energy storage device that uses carbon with a large surface area as its electrode [1,6-7]. Energy storage occurs based on the formation of ion and electron pairs that appear in the electrode/electrolyte interface [8]. These charges form in the microspores of carbon electrodes [9]. A carbon electrode with a high surface area is produced from the carbonization and activation of precursor material, such as biomass [2]. The use of various types of biomass as raw material in producing of carbon electrodes has been widely reported. Several papers have studied the synthesis of carbon electrodes from biomass materials, including palm oil [10], rice husks [11], corncob [12], apricot and peach stones [13], and rubber wood sawdust [14]. Farma *et. al* reported a carbon electrode made from empty fruit bunches of oil palm using a combination of physical and chemical activation. The surface area and specific capacitance of the electrode were found to be as high as 1704 m^2 g^{-1} and 150 F g^{-1}, respectively [10]. Teo *et. al* produced an electrode with a surface area as large as 2696 m^2 g^{-1} and a specific capacitance of 147 Fg^{-1} using a rice husk precursor [11]. Corncob was used as the raw material in supercapacitor production by Qu *et. al*. A surface area of 1210 m^2 g^{-1} and a specific capacitance of 314 F g^{-1} were obtained [12]. Huang *et. al* produced a supercapacitor electrode from apricot stone with a surface area of 1737 m^2 g^{-1} and a specific capacitance of 165 F g^{-1} [13]. These reports indicate that carbon material derived from agricultural residues possesses a large surface area and high specific capacitance. Other reports reveal that the search for a new biomass precursor from which to produce a superior carbon electrode continues. The use of biomass waste materials has also become an option in the effort to decrease the production cost of carbon electrodes. There are a number of reports on the use of waste materials, such as potato waste residue [3], waste particleboard [15], waste tea leaves [16], plant waste [17] and fallen leaves [18]. The surface area and specific capacitance of carbon electrodes whose raw materials are derived from waste range from 1000 m^2 g^{-1} to 3000 m^2 g^{-1} and 100 F g^{-1} to 330 F g^{-1}, respectively. Superior capacitive properties, large surface area and relatively low production cost represent advantages that continue to be sought in biomass used to synthesize carbon electrodes for supercapacitors. These advantages also informed our consideration of mission grass flowers as a raw material for the production of carbon electrodes. The mission grass flowers used here to create carbon monolith electrode were collected from the campus of Riau University, Pekanbaru, Indonesia. The monolith form offers another means to decrease the production cost of carbon electrodes by decreasing the cost of using an adhesive. This report describes the physical and electrochemical properties of a carbon electrode made from mission grass flowers based on several aspects: (1) carbonization temperature, (2) physical activation temperature, (3) chemical activation agent and (4) particle size. This paper demonstrates that mission grass flowers can be considered a potential candidate raw material for the manufacture of an activated carbon monolith for supercapacitor application.

2. EXPERIMENTAL SECTION

2.1 Electrode preparation

Twelve types of activated carbon monolith (ACM) made from the flowers of mission grass (FMG) were produced. The ACM synthesis followed our previously reported method [19]. The FMG samples were dried and subsequently pre-carbonized at 250 °C for 2.5 hours. The pre-carbonized samples were ground and then milled for 20 hours. A sieving process was conducted to obtain self-adhesive carbon grains (SACGs). The SACG samples were moulded into pellet form using a hydraulic press at a compression pressure of 8 metric tons. Carbon electrode sample variations were differentiated by (i) type and concentration of chemical activating agent such as $ZnCl_2$, NaOH and KOH in several concentration (0.3 M, 0.4 M, 0.5 M, and 0.7 M), (ii) physical activation (CO_2 temperature), (iii) carbonization temperature and (iv) particle size. The sample names and synthesis specifications are listed in Table 1. All ACMs were carbonized in a nitrogen gas environment with a constant flow rate of 1.5 L min^{-1} through a multilevel heating profile, as has been reported [20]. The physical activation was performed in CO_2 gas atmosphere for 2 hours. All electrodes were polished into a desired thickness of 0.3 mm. Subsequently, the ACMs were washed until the pH of the washing water became neutral (7).

Table 1. Sample codes and synthesis specifications.

Samples name	Syntheis spesification (chemical activating agent, CO_2 temperature for 2 hours, carbonization temperature and particles size)
ZC80K6	0.4 M $ZnCl_2$, 800 °C (2h) , 600 C, ≤53 μm
ZC85K6	0.4 M $ZnCl_2$, 850 °C (2h), 600 C, ≤53 μm
ZC90K6	0.4 M $ZnCl_2$, 900 °C (2h), 600 C, ≤53 μm
NC85K5	0.4 M NaOH, 850 °C (2h), 500 C, ≤53 μm
NC85K6	0.4 M NaOH, 850 °C (2h), 600 C, ≤53 μm
NC85K7	0.4 M NaOH, 850 °C (2h), 700 C, ≤53 μm
NC85K8	0.4 M NaOH, 850 °C (2h), 800 C, ≤53 μm
K3C85K6	0.3 M KOH, 850 °C (2h), 600 C, ≤53 μm
K5C85K6	0.5 M KOH, 850 °C (2h), 600 C, ≤53 μm
K7C85K6	0.7 M KOH, 850 °C (2h), 600 C, ≤53 μm
$NC85K6P_A$	0.4 M NaOH, 850 °C (2h), 600 C, ≤38 μm
$NC85K6P_B$	0.4 M NaOH, 850 °C (2h), 600 C, 39-52 μm

2.2. Physical properties

The crystal structure of the carbon electrode was analysed using the X-ray diffraction (XRD) method and an X-Pert Pro. Measurements were conducted using Cu Kα 15.406 nm as a radiation source. The measurement was performed in a diffraction angle (2θ) range of 10-100°. The characteristics of angle 2θ were analysed using Microcal Origin software. Interlayer spacing (d_{hkl}) was investigated using the Bragg equation ($n\lambda = 2\ d \sin 2\theta$). The microcrystallite dimensions (L_c and L_a) were calculated using the Debye-Scherrer equation ($L_a=1.94\ \lambda/\beta \cos\theta_{(100)}$ and L_c= 0.89

$\lambda/\beta \cos\theta_{(002)}$), where L_a and L_c the microcrystallite dimensions in Å, λ is the wavelength in Å, β is the bandwidth in degrees, d_{100} is the diffraction angle on the reflecting planes hkl 100 in degrees and $d_{002}$is the diffraction angle on the reflecting planes hkl 002 in degrees. The porosity parameters were analysed using theisotherm adsorption and desorption of nitrogen gas at a temperature of 77.3 K using a Quantachrome Instruments device, version 11.0. Specific surface area and pore volume were calculated using the Bruenauer-Emmett-Teller (BET) method. The surface morphology of the ACMs wasexamined using scanning electron microscopy (SEM), and the elements contained in the electrode were analysed using energy dispersive X-rays (EDX) (Hitachi).

2.3. Cell fabrication and electrochemical properties

Supercapacitor cells are arranged in the form of a sandwich that consists of two electrodes, two current collectors, a separator and an electrolyte. The electrodes that were used were activated carbon monoliths manufactured from mission grass flowers. The current collector was a 316L stainless steel foil. The separator was duck eggshell membrane, as has been reported [21]. In addition, 1 M H_2SO_4 was used as an electrolyte. The electrochemical performance was assessed bycyclic voltammetry using a handmade instrument (Physic UR CV Rad-Er 5841) and calibrated using a Solatron 1280 instrument. The measurements were conducted at a scan rate of 1 mV s^{-1} and a potential window of 0-500 mV, which was controlled using cyclic voltammetry software CVv6. The specific capacitance was calculated using Equation 1:

$$C_{sp} = \frac{[I_c - I_d]}{s \; x \; m} \quad (1)$$

where I_c = charge current, I_d = discharge current, s = scan rate and m = electrode mass.

3. RESULTS AND DISCUSSION

3.1. Physical properties

The X-ray diffractogram results for representatives of the entire series of electrodes are shown in Figure 1. ZC80K6, ZC90K6, NC85K5, NC85K8 K3C85K6 and K7C85K6 series are presented in the two representative samples. The data reveal the relationship between the diffraction intensity and the scattering angle (2θ). Each curve reveals the presence of broadening peaks and sharp peaks. The broadening peaks clearly emerged in the diffraction angle ranges of 24-26° and 44-47°, which correspond to the reflecting planes of (002) and (100) that are representative of the amorphous structure of carbon material.

The higher intensity indicated that carbon is the primary component among the constituent materials of the samples. In addition, a broadening peak also appears at a diffraction angle of 80°, although with a relatively small intensity. Sharp peaks were observed in all samples, with relatively low intensities. These sharp peaks indicate that crystalline material was present in the sample. The relatively low scattering intensity indicates that the crystalline material occurred in a small percentage, i.e., as impurities in the carbon sample. The presence of crystalline material in carbon samples derived

from biomass materials is typically due to imperfect washing. One impurity present in carbon from biomass material is silica.

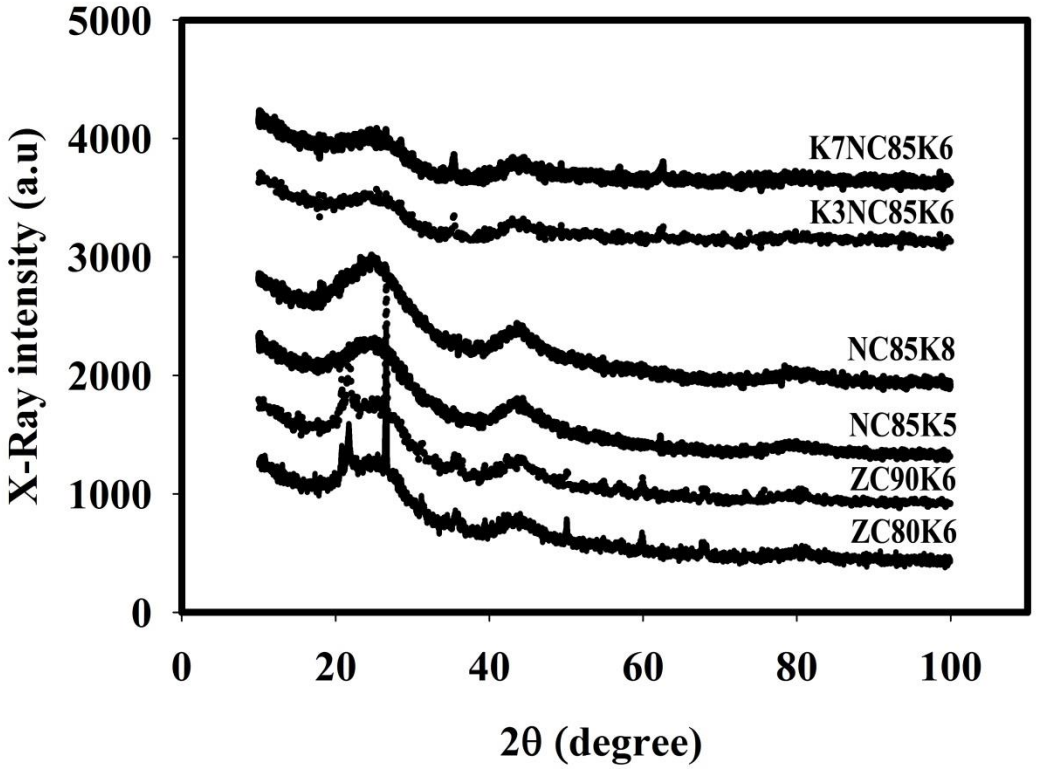

Figure 1. XRD curves for ZC80K6, ZC90K6, NC85K5, NC85K8 K3C85K6 and K7C85K6.

Table 2 shows several parameters of the samples, such as peak scattering angle (2θ), interlayer spacing (d), streak height (L_c) and steak width (L_a), the L_a and L_c ratio and N or L_c/d_{002} for all diffraction curves. The chemical activation treatment caused a shift in the diffraction angle of samples NC85K5, NC85K8, K3C85K6 and K7C85K6. Activation using NaOH and KOH resulted in diffraction angles thatdo not differ substantially from those of samples NC85K5, NC85K8, K3C85K6 and K7C85K6. The use of different chemical activators did not cause a significant change in d_{002}. The increase in the activation temperature of CO_2 in the ZCsK6 series resulted in d_{002} values that are nearly identical. The CO_2 activation temperature of the NC85Ks and KsC85K6 samples resulted in d_{002} parameters that are not identical. Table 2 shows the differences between the microcrystalline dimensions of L_c and L_a. The chemical activation of the NC85Ks and KsC85K6 series samples exhibits generally narrowing L_c and L_a. The higher activation temperature of CO_2 in the ZCsK6 series sample narrowed the values of L_c and L_a, which were not substantially different. Increasing the carbonization temperature in the NC85Ks series samples expanded L_c and narrowed L_a significantly. The increase in activator concentration in the KsC85K6 series sample resulted in slightly expanded L_c and slightly narrowed L_a. That is, this study reveals that the CO_2 activation temperature can affect the L_c value and that the selection of carbonization temperature affects the L_a. The results in Table 1 can be further analysed with respect to the L_c/L_a ratio and L_c/d_{002} (N_p). The chemical activation treatment

ofthe NC85Ks and KsC85K6 series samples generally resulted in an increase in the L_c/L_a ratio but did not indicate a trend for the N_p value. The higher CO_2 activation temperature of the ZCsK6 series samples revealed a reduced trend of the L_c/L_a ratio and N_p. The higher carbonization temperature of the NC85Ks series sample caused an increase in the L_c/L_a ratio and N_p. The increase in the activator concentration in the KsC85K6 series sample did not result in significant changes in the L_c/L_a ratio and N_p.

Table 2. Diffraction angles, interlayer spacing, crystallite dimensions, L_c/L_a ratios and surface area for all samples

Samples	$2\theta_{002}$ (^{0})	$2\theta_{100}$ (^{0})	d_{002} (Å)	d_{100} (Å)	L_c (Å)	L_a (Å)	L_c/L_a (Å)	N_p	S_{BET} ($m^2\ g^{-1}$)
ZC80K6	25.852	44.152	3.444	2.050	18.290	24.344	0.751	5.311	497
ZC90K6	25.833	45.761	3.446	1.981	11.558	24.566	0.470	3.354	773
NC85K5	24.933	44.790	3.568	2.022	10.980	20.377	0.539	3.077	937
NC85K8	24.960	45.349	3.565	1.998	12.743	11.617	1.097	3.574	765
K3C85K6	24.697	46.930	3.602	1.956	12.056	8.723	1.382	3.347	870
K7C85K6	24.748	46.632	3.594	1.946	11.158	8.472	1.317	3.104	723
NC85K6P_A	*	*	*	*	*	*	*	*	607
NC85K6P_B	*	*	*	*	*	*	*	*	956

The XRD analysis data presented in Table 2 were compared with the results from previous studies. The comparison revealed that the crystallinity properties of the monolithic carbon electrodes created from mission grass flowers occupy nearly the same region as those of carbon electrode materials created from another biomass. For example, for a series of monolithic carbon electrode samples made from coffee endocarp, it was found that d_{002}, L_c, L_a and L_c/L_a were in a range of 3.4-3.8 Å, 10-16 Å, 23-42 Å, 0.31-0.67 and 2-4.7, respectively [22]. For monolithic carbon electrodes from oil palm empty fruit bunches, Farma *et. al* obtained d_{002}, d_{100}, L_a, L_c and L_c/L_a as high as 3.69-3.71 Å, 2,068-2,086 Å, 8-10 Å, 48-52Å, 0.162-0.217 and 2.29-2.8, respectively [10]. Our results for a series of carbon electrode samples made from mission grass flowers for d_{002}, d_{100}, L_a, L_c and L_c/L_a were 3.44-3.6 Å, 1.94-2.05 Å, 11.15-18.29 Å, 8.4-24.56 Å, 0.47-1.38 and 3.07-5.31, respectively. These results indicate that the carbonization and activation processes that were performed resulted in a microcrystallite size and orientation that affected the capacitive properties of the supercapacitor cell.

Isothermal N_2 adsorption was performed on a small number of representative samples from each series using Quanta chrome Instruments device. Surface area calculations were only performed for 0.3 relative pressures. The specific surface area (S_{BET}) is shown in Table 2. The data in Table 2 were evaluated according to several aspects, such as (i) chemical activation, (ii) physical activation using CO_2 gas and (iii) differences in carbonization temperature. Chemical activation generally produced higher S_{BET}. The NC85Ks, KsC85K6 and ZCsK6 series samples were in order porosity properties of the sample from the higher to lower in the series sample. The use of NaOH as an activating agent in the NC85Ks sample series obtained higher S_{BET} than the KOH activating agent in the KsC85K6 sample series.

The addition of the KOH concentration in the KsC85K6 sample series decreased the S_{BET}. The increase in the concentration of a chemical activator was expected to develop a new pore structure. An increase in the concentration of KOH activators in a relatively low percentage has also been reported to increase the surface area of activated carbon samples created from olive residual [23]. The higher CO_2 activation temperature in the ZCsK6 series samples produced an increase in S_{BET}. That is, clearly CO_2 activation can develop new pores. Taer *et. al* reported that increasing the CO_2 activation temperature from 800 to 900 °C for carbon electrode samples from rubber wood sawdust increased the sample's S_{BET} from 390 to 683 $m^2 g^{-1}$ [19]. The higher carbonization temperature in the NC85Ks series decreased the S_{BET}. Du et al reported that samples of carbon electrodes created from ramie that was impregnated with $ZnCl_2$ and carbonized at temperatures from 400-750 °C exhibited decreased surface area. The S_{BET} of the sample linearly decreased from 2087 to 1592 $m^2 g^{-1}$ [24]. Apricot peels that were chemically activated using NaOH and then carbonized at 400-800 °C also exhibited decreased reduce the surface area: the S_{BET} decreased from 2335-1342 $m^2 g^{-1}$ [25]. Similar results were reported for activated carbon made from particleboard, whereby the surface area decreased from 1190 to 849 $m^2 g^{-1}$ when the carbonization temperature was increased from 400 to 600 °C [26]. The increase in temperature carbonization caused the pore size to become larger. Therefore, the specific surface area decreased. The S_{BET} is an important factor in the production of high-performance carbon electrodes. In this study, the effect of uniform particle size on the NC85K6Px series was investigated. The NC85K6P_B samples produced S_{BET} and V_{STP} that were higher than in NC85K6P_A. The NC85K6P_B samples also produced S_{BET} that was higher than in NC85K5. In this study, uniform particle size was expected to develop the pore structure and modify the surface area of the carbon electrode material.

Characterization of the surface morphology of the carbon electrode was performed using scanning electron microscopy (SEM). SEM data were collected for the NC85K6 and NC85K6P_B samples (Figure 2).

The NC85K6P_B samples appeared to possess a more uniform particle shape with a space between the larger particles (Figure 2a). Figure 2b shows the arrangement of particles for sample NC85K6. The constituent particles of this sample do not appear to be uniform and are arranged more densely. This outcome was caused by decreasing the homogeneity of the particles. Thus, smaller particles fill in the spaces between larger particles. The SEM data clearly support the results for electrochemical properties, particularly those shown in Figure 2d, where the space between the particles in the NC85K6P_B samples is associated with the smooth process of ion diffusion into the micropores on interface of the carbon particles. Figure 2c and 2d present magnifications of Figure 2a and 2b, respectively. The SEM results also indicate the presence of other materials in addition to the carbon found in both samples. These other materials are indicated by small white particles.

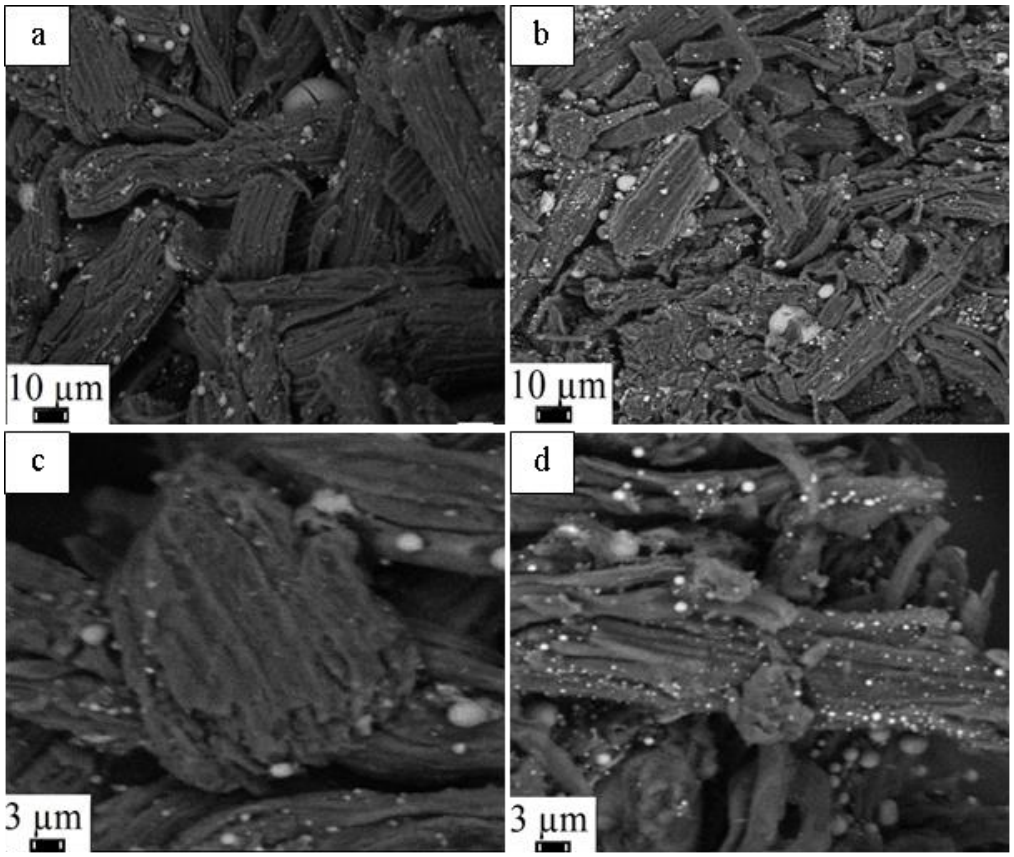

Figure 2. SEM micrographs for a) NC85K6PB in 1000 mag, b) NC85K6 in 1000 mag, c) NC85K6PB in 1500 mag and d) NC85K6 in 1500 mag

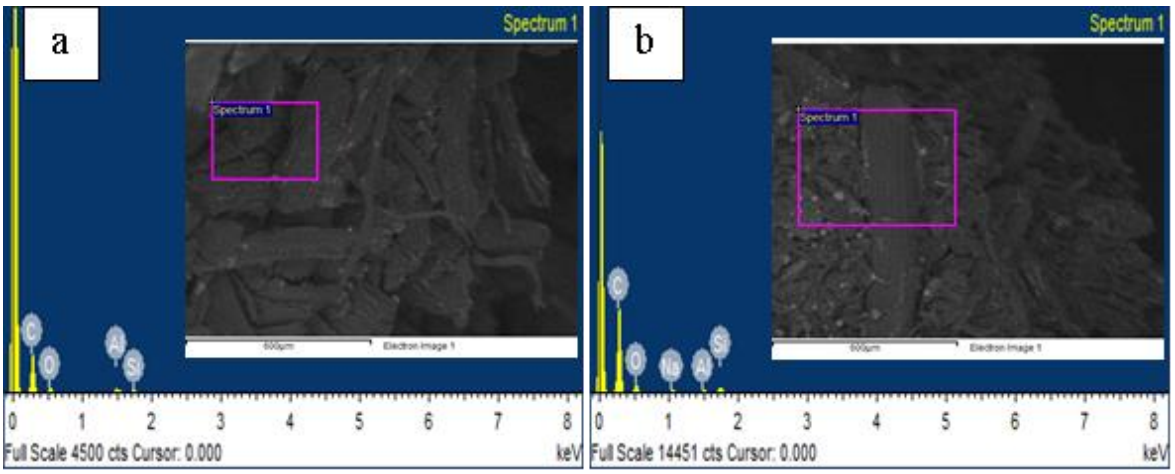

Figure 3. EDX spectrum for a) NC85K6PB and b)NC85K6

The element content of the samples was investigated using the energy dispersive X-ray (EDX) method. The EDX spectra are shown in Figure 3. The quantitative data for the spectra are provided in Table 3 and indicate that the sample consists of approximately 77% carbon. The level of homogeneity of particle size affected constituent element composition across the various samples. The NC85K6P_B samples have more homogenous particles and therefore present a larger number of oxygen bonds than

NC85K6. Thus, the carbon content is smaller. A decrease in the homogeneity of the particles that compriseNC85K6 indicates a large number of other materials in addition to the carbon compared to NC85K6P_B. This outcome was caused by smaller pore size, which can "catch" other materials (in addition to the carbon) that are not removed during the heating and washing process.

Table 3. EDX element percentages for NC85K6PB and NC85K6

Element	Weight%	
	NC85K6P_B	NC85K6
C K	72.57	76.65
O K	19.07	17.12
Na K	-	1.57
Al K	4.88	1.42
Si K	3.48	3.24
Totals	100.00	100.00

3.2. Electrochemical properties

The cyclic voltammetry data for all supercapacitor cells are shown in Figure 4. Figure 4a shows the CV curve for the ACMs that were synthesized with a NaOH chemical activator and carbonized at 500 °C, 600 °C, 700 °C and 800 °C. The CV curve represents current density vs voltage relations. All the data are similar but have differences in the width of the area in which current is charged and discharged. The differences in this area appear more clearly on the half width of the potential window, i.e., on potential 2.5 V. The higher carbonization temperatures were found for the lower charge and discharge current density. The decrease in the value of these currents was influenced by the decrease in the specific surface areas of the ACM samples. The specific surface areas of an electrochemical double-layer capacitor system influence the number of ions that can diffuse into the porous structures of the ACM electrodes to form ion-electron pairs [27]. Figure 4b shows the capacitive properties of the supercapacitor cells that were produced from the electrodes that were synthesized via chemical activation using a KOH activating agent.

These samples were varied using KOH concentrations of 0.3, 0.5 and 0.7 M and labelled as the KsC85K6 series. The curve form for the KsC85K6 samples clearly seems differs from that of the NC85Ks series. The chemical activation treatment in the synthesis of carbon electrodes in the KsC85K6 series produced a CV curve with a nearly rectangular form. The different KOH concentrations of the samples of the KsC85K6 series resulted in CV curves that were highly similar with slight differences in current value. The difference in KOH activator concentration resulted in the development of a micropore structure in the supercapacitor cell electrode [28]. Differences between chemical activators also resulted in different CV curve shapes in other studies [29]. The differences in the shape of the CV curve correspond to different pore forms and distributions for different chemical activators [23]. Figure 4c represents supercapacitor cells that were constructed using activated carbon electrodes with different particle sizes. Differences in the size of the constituent particles seem to produce the different CV curve shapes. The larger particles of the NC85K6P_B samples series produced

a CV curve with larger I-V areas than the smaller particle size of sample NC85K6P$_A$.

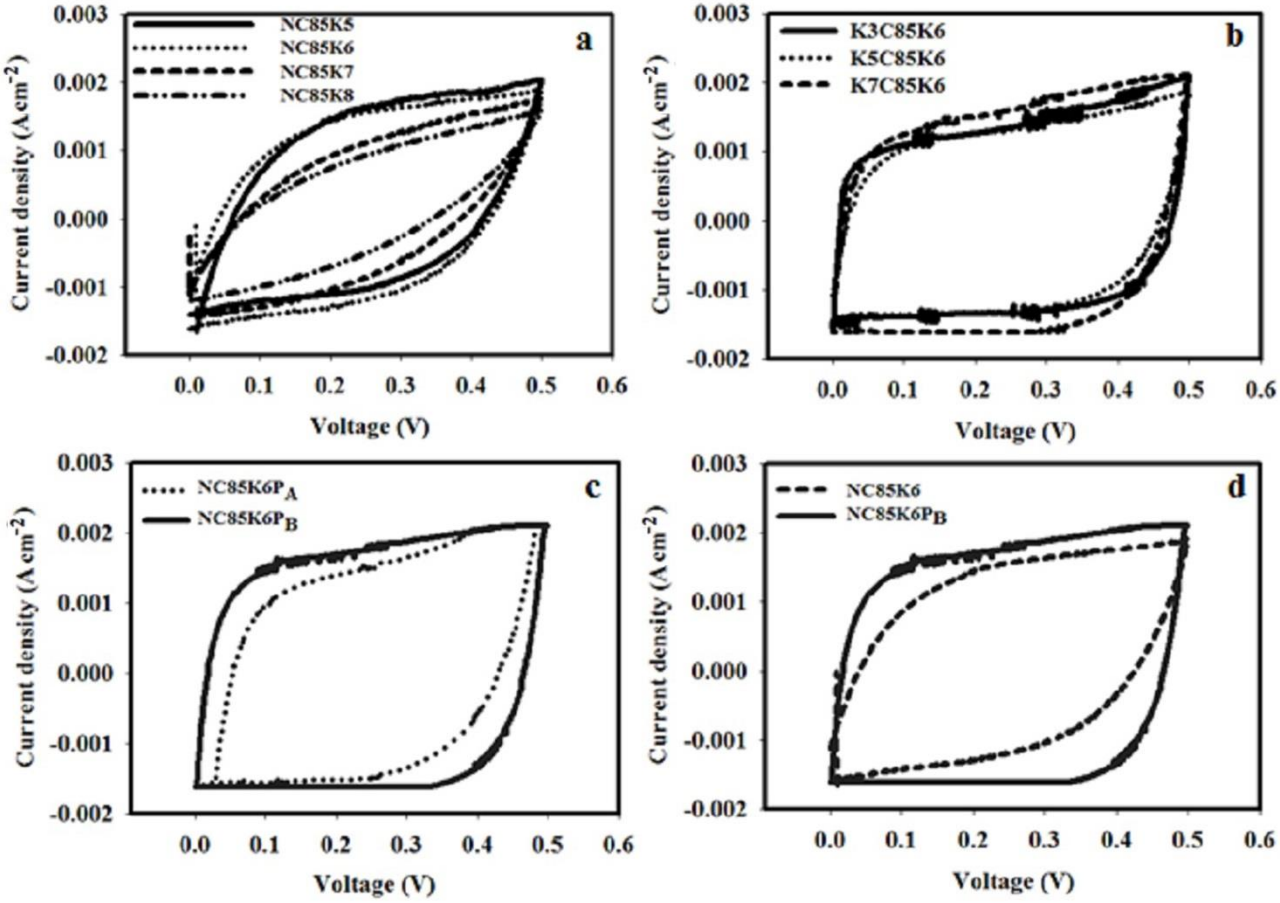

Figure 4. CV data obtained at a scan rate of 1 mVs^{-1} for a) NC85Ks, b) KsC85K6, c) NC85K6Px and d) the homogeneity level of particles for the various CV curves

These results correlate with the specific surface area data for sample NC85K6P$_B$, whose surface area is larger than in sample NC85K6P$_A$ (Table 2). The larger particle size of the NC85K6P$_B$ samples also resulted in larger pores between particles than in NC85K6, which caused the large number of ion transfers into the samples. Uniform particle size resulted in the different shape CV curve in Figure 4d. This figure shows CV data for two supercapacitor cells that were constructed from electrodes with homogenous particle sizes: in the range of 39-52 microns for the NC85K6P$_B$ samples and less than 52 microns for the NC85K6 samples. Modification of particle-size homogeneity resulted in the expansion of the I-V area in the CV curve of the NC85K6P$_B$ samples. The differences in these homogeneity properties resulted in different numbers of spaces between particles. Decreasing the homogeneity of sample NC85K6 produced less ion transfer than in NC85K6P$_B$, which occurred because the smaller particles covered the spaces between particles such that the number of pores between particles and the surface areas were decreased.

The specific capacitance values (C_{sp}) for all of the supercapacitor cells were evaluated using Formula 1. The C_{sp} values for all of the sample series are shown in Table 4. Increasing the CO_2 activation temperature increased the C_{sp} values in the ZCsK6 series. It seems that the best activation

temperature was 900 °C. CO_2 activation temperature plays an important role in generating optimum pore properties. Previous reports have demonstrated the optimum conditions for activating carbon electrodes created from various biomass materials and the optimum capacitances, e.g., for capacitor electrodes produced from rubber wood sawdust [19] and a mixture of apricot and peach stones [13]. Chemical activation treatment can generally increase C_{sp} values. The higher carbonization temperature in the sample series NC85Ks decreased C_{sp}. Thus, it seems the suitable carbonization temperature is 500-600 °C. Similar trends were observed in another study [24]. The chemical activation treatment using KOH in the KsC85K6 series obtained higher C_{sp} than in the NC85Ks series. Increasing the KOH concentration in the KsC85K6 series increased the C_{sp} values. Increasing the particle size in the NC85K6P_B sample obtain a higher C_{sp} value than in the NC85K6$P_A$sample. Particle size uniformity also affects the capacitance properties of supercapacitor cells. The entire correlated calculation of the specific capacitance values of Figure 4 is shown in Table 4.

Table 4. Specific capacitance, energy and power for all samples.

Samples	C_{sp} (F g^{-1})	E (Wh kg^{-1})	P (W kg^{-1})
ZC80K6	81	0.63	33.63
ZC85K6	87	0.73	32.30
ZC90K6	93	0.83	36.22
NC85K5	95	0.66	35.71
NC85K6	81	0.65	28.31
NC85K7	58	0.52	25.36
NC85K8	39	0.35	21.72
K3C85K6	81	0.70	31.70
K5C85K6	88	0.76	35.01
K7C85K6	100	0.87	32.69
NC85K6P_A	87	0.75	30.45
NC85K6P_B	121	0.97	36.22

The density of energy and power for all of the supercapacitor cells is also shown in Table 4. The suitable CO_2 activation temperature increased the energy in the ZCsK6 series. However, increasing the activation temperature did not exhibit a clear trend with respect to power density. A comparison of chemical activation treatments did not display a clear trend with respect to changes in the density of energy and power. Increasing the carbonization temperature in the NC85Ks series decreased energy and power. The chemical activation treatment using KOH in the KsC85K6 series produced higher energy than in the NC85Ks series and did not exhibit a general trend with respect to the change in power density. Increasing the concentration of KOH activators in the KsC85K6 series increased the energy density but did not display a general trend with respect to the change in power density. The larger particle size one of the NC85K6P_B sample produced higher energy density and power density compared to the NC85K6P_A sample. In this study, in which the combination of specific capacitance, high energy and power were expected to generate a high-performance supercapacitor cell, it seems that the selection of a combination of physical and chemical activation produced higher performance. In the chemical activation process, the selection of the materials of chemical activation

and concentration is important. An appropriate temperature during carbonization and physical activation are also factors that determine supercapacitor cell performance. An important finding in this study is that the size and degree of homogeneity of the constituent particles of the carbon materials are highly important to generate a high-performance supercapacitor cell. This study demonstrates that a particle size in the range of 39-52 μm contributes importantly to generating supercapacitor cells with good performance.

Based on the preceding analysis, the physical properties (i.e., microcrystallite size and surface area) are clearly related to electrochemical properties (i.e., specific capacitances, energy density and power density). For example, samples with relatively small L_c result in a large surface area that is directly proportional to the specific capacitance of the supercapacitor cell [30]. These findings are evident in samples ZC90K6, NC85K5 and K7C85K6. L_c appears inversely proportional to surface area. The empirical relation of L_c and S_{BET} has been described using an empirical formula [31]. For each electrode, L_c is 11.55, 10.98 and 11,15 Å, and S_{BET} is 773, 937 and 723 $m^2\ g^{-1}$, respectively. The ZC90K6, NC85K5 and K7C85K6 samples also display relatively high capacitive properties in the supercapacitor cell, as high as 93,95 and 100 F g^{-1}, respectively. In contrast, for a sample with relatively L_c, a small surface area was found. For example, in the ZC80K6 and NC85K8 samples, L_c was 18.29 and 12,743 Å, and S_{BET} was 497 $m^2\ g^{-1}$ and 765 $m^2\ g^{-1}$, respectively. The capacitances of the supercapacitor cells for the corresponding electrodes were 81 F $g^{-1}$and 39 F g^{-1}, respectively. This finding clearly justifies the modification of the physical properties that were performed to alter the electrochemical properties of supercapacitor cells.

Table 5. Comparison of several biomass-based activated carbon monoliths for supercapacitor application according to specific capacitance, measurement technique and electrolyte used in cell characterization.

Biomass	C_{sp} (F. g^{-1})	Technique	Electrolyte	Reference
Bamboo shell	204	3 electrodes	1 M H_2SO_4	[32]
Coniferous pine	90	2 electrodes	1 M Na_2SO_4	[33]
Sugarcane bagasse	178	2 electrodes	1 M H_2SO_4	[21]
Patato waste residue	255	3 electrodes	2 mol L^{-1} KOH	[3]
Oil palm kernel shell	210	3 electrodes	1 M KOH	[34]
Fagus Silvatica	133	3 electrodes	1 M KOH	[35]
Tobacco stem	167	2 electrodes	1 mol Li_2SO_4	[36]
Coconut shell	350	3 electrodes	Acetonitrile	[37]
Oil palm empty fruit bunches	150	2 electrodes	1 M H_2SO_4	[10]
Cassava peel	29	2 electrodes	1 M H_2SO_4	[38]
Banana peel	68	2 electrodes	1 M H_2SO_4	[39]
Banana stem	170	2 electrodes	1 M H_2SO_4	[40]
Durian shell	88	2 electrodes	1 M H_2SO_4	[41]
Coconut husk	184	2 electrodes	1 M H_2SO_4	[42]
Sago waste	132	2 electrodes	1 M H_2SO_4	[43]
Rubber wood sawdust	151	2 electrodes	1 M H_2SO_4	[14]
Coffee endocarp	176	3 electrodes	1 M H_2SO_4	[22]
Mission grass	121	2 electrodes	1 M H_2SO_4	[recent study]

The literature describes the manufacture of activated carbon-based electrode supercapacitor cells from various types of biomass. Carbon supercapacitor electrodes fabricated from mission grass flowers were compared with carbon electrodes made from different biomass sources with respect to specific capacitance, measurement method and the electrolytes that were used. The results are summarized in Table 5. The specific capacitance of the samples appears in a range comparable to that of other sample supercapacitor electrodes. Differences in capacitance were clearly influenced by the measurement method and the type of electrolyte used. Measurement performed on a three-electrode cell indicated greater capacitance than measurement that used two electrodes. Different electrolytes differently affect the size of the ion used in the formation of charge pairs in the charge mechanism of a double-layer capacitor system. Other factors that may also affect capacitance differences include the activation process used in the preparation of carbon electrodes. Because each raw material may have been activated using a different method, the electrode will have different physical properties and relatively different capacitive properties. Over all, a carbon monolith electrode for a supercapacitor was successfully manufactured from mission grass flowers. The analysis demonstrated the potential capacitive properties of an electrode produced from this low-cost biomass source. Therefore, mission grass flowers can be recommended as a potential material to be developed into a carbon electrode for supercapacitor application.

4. CONCLUSION

Mission grass flowers clearly display an excellent combination of physical and electrochemical properties. The sample preparation process used to synthesize an activated carbon monolith based on carbonization temperature, physical activation temperature, the selection of a chemical activator and particle homogeneity produced a maximum specific surface area of 950 m^2 g^{-1} and a maximum specific capacitance of 121 F g^{-1}.

ACKNOWLEDGEMENTS
The author would like to thank the DRPM Kemenristek-Dikti through the third year Project of PDUPT with the title “Potential of Urban Solid Waste Utilization as a Supercapacitor Electrode” with contract number: 759/UN.19.5.1.3/PT.01.03/2019.

References

1. M. Inagaki, H. Konno, O. Tanaike, *J. Power Sources*, 195 (2010) 7880.
2. A. M. Abioye, F. M. Ani, *Renew Sust. Energ. Rev.*, 52 (2015) 1282–1293.
3. M. Ma, Q. Yang, K. Sun, H. Peng, F. Ran, X. Zhao, and Z. Lei, *Bioresour. Technol*., 197 (2015) 137.
4. S. Prasertwasu, D. Khumsupan, T. Komolwanich, T. Chaisuwan, A. Luengnaruemitchai, S. Wongkasemjit, *Bioresour. Technol.*, 163 (2014) 152.
5. E. Cardona, J. Rios, J. Pena, M. Penuela, L. Rios, *Biomass Bioenerg.*, 95 (2016) 206.
6. S. Faraji, F. N. Ani, *Renew. Sust. Energ. Rev*, 42 (2015) 823–834.
7. A. González, E. Goikolea, J. A. Barrena, R. Mysyk, *Renew. Sust. Energ. Rev.*, 58 (2016) 1189-1206.
8. R. Kötz, M. Carlen, *Electrochim. Acta*, 45 (2000) 2483.

9. A. Burke, *J. Power Sources*, 91 (2000) 37.
10. R. Farma, M. Deraman, A. Awitdrus, I. A. Talib, E. Taer, N. H. Basri, J. G. Manjunatha, M. M. Ishak, B. M. N. Dollah, S. A. Hashmi, *Bioresour. Technol.*, 132 (2013) 254.
11. E. Y. L. Teo, L. E. P. Ng. Muniandy, F. Adam, A. R. Mohamed, R. Jose, K. F. Chong, *Electrochim. Acta*, 192 (2016) 110–119.
12. W. H. Qu, Y.Y. Xu, A. H. Lu, X. Q. Zhang, W. C. Li, *Bioresour. Technol.*, 189 (2015) 285.
13. C. Huang, A. M. Puziy, T. Sun, O. I. Poddubnaya, F. Suárez-Garcıa, J. M. D. Tascón, D. Hulicova-Jurcakova, *Electrochim. Acta*, 137 (2014) 219.
14. E. Taer, M. Deraman, I. A. Talib, A. Awitdrus, S. A. Hashmi, A. A. Umar, *Int. J. Electrochem. Sci*, 6 (2011) 3301 – 3315.
15. T. X. R. Shang, Q. Ren, Y. M. Zhu, X. J. Jin, *Electrochim. Acta*, 163 (2015) 32.
16. C. Peng, X. B. Yan, R. T. Wang, J. W. Lang, Y. J. Ou, Q. J. Xue, *Electrochim. Acta*, 87, (2013) 401.
17. C. Chen, D. Yu, G. Zhao, B. Du, W. Tang, L. Sun, Y. Sun, F. Besenbacher, M. Yu, *Nano Energ*, 27 (2016) 377.
18. Y. P. Li, Y. T. Pi, L. M. Lu, S. H. Xu, T. Z. Ren, *J. Power Sources*, 299 (2015) 519.
19. E. Taer, M. Deraman, I. A. Talib, A. A. Umar, M. Oyama and R. M. Yunus, *Curr. Appl. Phys.*, 10 (2010) 1071.
20. E. Taer, M. Deraman, I. A. Talib, S. A. Hasmi, A. A. Umar, *Electrochim. Acta*, 56 (2011) 10217.
21. E. Taer, Iwantono, S. T. Manik, R. Taslim, D. Dahlan, M. Deraman, *Adv. Mater. Research*, 896 (2014) 179.
22. J. M. Valente-Nabais, J. G. Teixera and I. Almeida, *Bioresour. Technol*., 102 (2011) 2781.
23. E. Elmouwahidi, E. Bailón-García, A. F. Pérez-Cadenas, F. J. Maldonado-Hódar, F. Carrasco-Marín, *Electrochim. Acta*, 229 (2017) 219–228.
24. X. Du, W. Zhao, Y. Wang, C. Wang, M. Chen, T. Qi, C. Hua, M. Ma, *Bioresour. Technol*., 149 (2013) 31–37.
25. B. Xu, Y. Chen, G. Wei, G. Cao, H. Zhang, Y. Yang, *Mater. Chem. Phys.*, 124 (2010) 504.
26. X. J. Jin, M. Y. Zhang, Y. Wu, J. Zhang, J. Mu, *Indust. Crops Product.*, 43 (2013) 617.
27. V. .V N. Obreja, *Phys. Low-dimen. Syst. Nanostruc.*, 40 (2008) 2596.
28. R. L. Tseng, S. K. Tseng, F. C. Wu C. C. Hu, C. C. Wang, *J. Chin. Institute. Chem. Engineers*, 39 (2008) 37–47.
29. Y. Boyjoo, Y. Cheng, H. Zhong, H. Tian, J. Pan, V. K. Pareek, S. P. Jiang, J. F. Lamonier, M. Jaroniec, J. Liu, *Carbon*, 116 (2017) 490.
30. L. H. Wang, M. Toyoda, M. Inagaki, *New Carbon Mater*, 23 (2008) 111.
31. K. Kumar, R. K. Saxena, R. Kothari, D. K. Suri, K. Kaushik, J. N. Bohra, *Carbon*, 35 (1997) 1842.
32. B. Lu, L. Hu, H. Yin, X. Mao, W. Xiao, D. Wang, *Int. J. Hydrogen Energy*, 41 (2016) 18713.
33. N. Manyala, A. Bello, F. Barzegar, A. A. Khaleed, D. Y. Momodu, J. K. Dangbegnon, *Mater. Chem. Phys*., 182, (2016) 139.
34. I. I. Misnon, N. K. M. Zain, R. A. Aziz, B. Vidyadharan, R. Jose, *Electrochim. Acta*, 174 (2015) 78.
35. A. Gutiérrez-Pardo, J. Ramírez-Rico, R. Cabezas-Rodríguez and J. Martínez-Fernández, *J. Power Sources*, 278 (2015) 18.
36. P. Kleszyk, P. Ratajczak, P. Skowron, J. Jagiello, Q. Abbas, E. Frackowiak, F. Beguin, *Carbon*, 81 (2015) 148.
37. M. Galinski, K. Babe, K. Jurewicz, *J. Power Sources*, 228 (2013) 83-88.
38. E. Taer, Iwantono, M. Yulita, R. Taslim, A. Subagio, Salomo, M. Deraman, *AIP. Conf. Proc.*, 1554 (2013) 70.
39. E. Taer, R. Taslim, Z. Aini, S. D. Hartati, W. S. Mustika, *AIP Conf. Proc*., 1801 (2017) 040004-1

40. E. Taer, R. Taslim, W. S. Mustika, B. Kurniasih, Agustino, A. Afrianda, Apriwandi, Int. J. Electrochem. Sci., 13 (2018) 8428
41. E. Taer, P. Dewi, Sugianto, R. Syech, R. Taslim, Salomo, Y. Susanti, A. Purnama, Apriwandi, Agustino, R. N. Setiadi, AIP Conf. Proc., 1927 (2018) 030026-1
42. E. Taer, R. Taslim, A. W. Putri, A. Apriwandi, A. Agustino, *Int. J. Electrochem. Sci.*, 13 (2018) 12072.
43. E. Taer, A. Afrianda, Apriwandi, R. Taslim, A. Agustino, Awitdrus, R. Farma, *Int. J. Electrochem. Sci.*, 13 (2018) 10688.